Chemical Engineering Journal 428 (2022) 131106

Contents lists available at ScienceDirect

Chemical Engineering Journal

journal homepage: www.elsevier.com/locate/cej

Bed packing configuration and hot-spot utilization for low-temperature CO_2 methanation on monolithic reactor

Huong Lan Huynh [a], Wakshum Mekonnen Tucho [b], Qi Shen [c,*], Zhixin Yu [a,*]

[a] Department of Energy and Petroleum Engineering, University of Stavanger, Stavanger 4036, Norway
[b] Department of Mechanical and Structural Engineering and Material Science, University of Stavanger, Stavanger 4036, Norway
[c] Institute of New Energy, School of Chemistry and Chemical Engineering, Shaoxing University, Shaoxing 312000, China

ARTICLE INFO

Keywords:
CO_2 methanation
Hot-spot
Bed packing
Monolithic reactor
Low-temperature

ABSTRACT

The revival of CO_2 methanation (Sabatier reaction) as part of the large-scale Power-to-Gas technology has stimulated the development of novel reactor concepts for better heat management due to its exothermic nature. The generation of hot-spots in fixed bed reactors could reduce methane yield, accelerate catalyst deactivation, and potentially cause thermal runaway. However, hot-spots could be utilized to achieve outstanding CO_2 methanation performance at low temperatures and high gas flow rate in monolithic reactors, whereas strategic bed packing configurations could boost the performance of low-activity catalytic beds. We prepared NiFe catalysts derived from in-situ grown layered double hydroxides via urea hydrolysis on washcoated cordierite honeycomb substrate with varying activities. Temperature profiles by both experimental and computational fluid dynamic (CFD) studies revealed hot-spot formation along catalytic beds. Hot-spots increased the catalytic beds' temperature due to high thermal conductivity of cordierite monolith, thus accelerated the reaction. The monolithic reactor with a single-monolith bed exhibited a methane yield of 16.5% at 250 °C, which was significantly increased to 80.4% on the reactor with three-monolith bed of the same catalyst at similar reaction condition with a constant ratio of catalyst mass to gas flow rate. A combined low-high activity monolithic bed was proposed which demonstrated high methane yield and excellent stability. Interestingly, the methane yields were higher at a gas flow rate of 1500 mL/min than that at 500 mL/min, again ascribed to the beneficial effect of hot-spot formation on monolithic reactors. Therefore, strategic bed packing configuration plays an important role in the optimization of monolithic methanation reactors, and hot-spot formation could be exploited to achieve excellent CO_2 methanation performance at low temperatures.

1. Introduction

Discovered more than one hundred years ago by Nobel laureate Paul Sabatier, CO_2 methanation reaction which converts carbon monoxide (CO) or carbon dioxide (CO_2) and hydrogen (H_2) into methane (CH_4) is one of the most important chemical reactions for heterogeneous catalysis research [1,2]. It has been used as an important purification step to remove traces of CO and CO_2 from H_2-rich gases for ammonia production, for example. Recently, renewed interest in methanation has been driven by the energy transition towards renewable sources, e.g., solar and wind power [3]. As renewable energies become an important part of the transitional energy system, the inherent intermittency of wind and solar power has appeared to be problematic since it affects the balance between energy supply and demand. Power-to-Gas (PtG) technology has been proposed as a promising solution for large-scale energy storage of renewable electricity, in which CO_2 methanation is an important process [4,5]. The concept aims to use surplus renewable electricity to produce hydrogen via water electrolysis. The green hydrogen is further reacted with carbon dioxide to produce synthetic natural gas (SNG).

$$CO_2 + 4H_2 \leftrightarrow CH_4 + 2H_2O,\ \Delta H_{298K} = -165.0\ \text{kJ/mol} \quad (1)$$

The Sabatier reaction (Equation. (1)) is thermodynamically favored at low temperatures and high pressures. However, it is difficult to obtain high conversion at low temperatures of 200–350 °C due to kinetic limitations. Thus, supported catalysts such as noble metals (e.g., Ru, Rh) or earth-abundant metals (e.g., Ni, Fe, Co) are applied in the process. Because of affordable cost and good catalytic performance, Ni-based catalysts are widely used in most industrial applications [6,7]. The

* Corresponding authors.
E-mail addresses: zhixin.yu@uis.no (Q. Shen), zhixin.yu@uis.no (Z. Yu).

https://doi.org/10.1016/j.cej.2021.131106
Received 5 May 2021; Received in revised form 15 June 2021; Accepted 28 June 2021
Available online 3 July 2021

Sabatier reaction is highly exothermic thus a large amount of heat could be generated during large-scale PtG process. This would cause hot-spots inside the reactor and potentially lead to thermal runaway. In addition, the CO_2 conversion and CH_4 selectivity will be reduced [8]. It has been reported that a temperature spike of 227 °C was recorded in an annular fixed-bed reactor filled with commercial Ni/Al_2O_3 trilobes catalysts during CO_2 methanation at an operating temperature of 225 °C, pressure of 0.4 MPa and gas hourly space velocity (GHSV) of 6000 h^{-1} [9]. Although a high methane yield of 83% was obtained, hot-spot formation appears to be the big challenge that should be tackled by proper reactor heat management.

New reactor concepts are focusing on improving the heat management of reactors in two-phase systems such as wall-cooled fixed bed, fluidized bed, coated honeycombs, or three-phase systems such as bubble column [10]. One of the most recent strategies to improve the methanation performance is the introduction of monolithic honeycomb catalysts. Structured reactors have the advantage of low pressure drop due to the channeling nature. The tunable thickness of catalyst layer which affects the diffusion length could be beneficial to optimize the efficiency of the catalysts. Moreover, high volumetric flow rates of feed gases can be handled by structured reactors with improved heat and mass transfer, especially for better heat transfer since monolithic substrates typically have good thermal conductivity [11]. There has also been an increasing application of structured catalysts and reactors for CO_2 methanation. For instance, Fukuhara *et al.* reported that under similar methanation conditions, honeycomb-type catalytic bed showed a flat temperature profile while granular-type catalytic bed showed a temperature rise of 20 °C due to poor heat dissipation of the conventional fixed bed [12]. However, at a higher gas flow rate, hot-spot formation was observed on the honeycomb monolithic bed. Great efforts to further improve heat and mass transfer along the monolithic bed have been devoted [13,14]. It was found that a less severe hot-spot formation could be obtained while high CO_2 conversion and CH_4 selectivity were maintained on a multi-stacked catalyst bed [15]. The researchers have been innovative by designing the bed packing configuration containing a sequence of coated and uncoated Ni/CeO_2 aluminum honeycomb-fin monolithic catalysts. Thus, the catalytic activity was discretely distributed along the reactor bed length which resulted in an optimal heat transfer and reaction rate. Kosaka *et al.* has recently reported that an increasing catalytic activity along the tubular catalyst bed could also prevent hot-spot formation compared to the uniform catalytic bed [16,17]. However, it was not anticipated that the performance of the low-activity catalysts was boosted by the observed hot-spots. Apparently, controlled hot-spot formation could be utilized for a more sustainable catalytic process and has been deliberately employed in certain reactor designs [18,19]. Therefore, it is important to fundamentally understand the effect of catalytic activity along the catalytic bed on the reactor temperature profiles.

We have recently developed a novel, highly reproducible and easily scalable synthesis procedure to prepare NiFe catalysts derived from layered double hydroxides (LDHs) precursors on cordierite (ceramic) honeycomb substrate [20]. The bimetallic honeycomb catalysts have shown excellent performance in CO_2 methanation. In this study, the preparation parameters were optimized to obtain honeycomb catalysts with different activities. We studied the effect of metal concentrations on catalyst loading and its performance in CO_2 methanation. The temperature profiles of the structured reactor packed with monolithic catalysts were investigated. Hot-spot formation was detected on the catalytic bed during CO_2 methanation at different operating temperatures and gas flow rates. We then investigated the effect of bed packing configurations on the formation of hot-spot and the overall CO_2 methanation performance. A computational fluid dynamic (CFD) model was developed to verify the experimental results. Long-term stability tests were also carried out to evaluate the monolithic catalysts for industrial applications of PtG technology. To the best of our knowledge, this is the first study to report CO_2 methanation on ceramic honeycomb monolithic reactors with different bed packing configurations.

2. Experimental

2.1. Catalyst preparation

The preparation method has been adapted from our previous work [20]. The honeycomb cordierite substrates (Applied Ceramics Inc., USA) were cylindrical with an outer diameter of 19 mm and a length of 20 mm. It consists of 230 cells per square inch (cpsi) with a channel wall thickness of 200 ± 50 μm. Prior to the synthesis steps, the substrates were washed with ethanol and distilled water and dried at 90 °C overnight. In order to increase the surface area, the ceramic substrates were dip-coated with alumina colloidal (Alfa Aesar, 20 wt% suspensions in water, particle size of 50 nm) three times with subsequent drying to obtain a washcoated layer with 14 wt% alumina. The washcoated substrate was calcined at 600 °C for 6 h with a heating ramp of 2 °C/min.

For the formation of NiFe-CO_3 LDHs, aqueous stock solutions consisting of nickel (II) nitrate hexahydrate, iron (III) nitrate nonahydrate, and urea (all from Merck Millipore) with total molar concentrations from 0.05M to 2M were used. The molar ratio between urea and total metal ion of Ni^{2+} and Fe^{3+} was 9.9 while the Fe^{3+}/Ni^{2+} molar ratio was kept constant at 0.25. The washcoated honeycomb was then immersed in a 45-mL stock solution contained by a Teflon-lined hydrothermal autoclave. Urea hydrolysis was carried out at 110 °C for 24 h. Subsequently, the obtained monolith was washed, dried, and calcined at 600 °C for 6 h with a ramp rate of 2 °C/min. The final monoliths are denoted as COR-*x*M, where *x* is the total metal concentration during preparation.

To characterize the as-prepared NiFe-CO_3 LDHs precursors, the solid precipitate in the autoclave after urea hydrolysis was collected, washed, and dried. These LDHs powders are named LDH-*x*M, where *x* is also the total metal concentration. The dry LDHs powders were calcined at similar conditions as the monolithic catalysts.

2.2. Catalyst characterization

X-ray diffraction (XRD) diffractograms of the LDHs powder precursors were recorded using D8 Advance micro-diffractometer (Bruker) equipped with CuKα radiation. The scanning speed was 1°/min over a 2θ range from 5° to 70°.

Temperature programmed reduction (TPR) of the calcined precursors was carried out on Autochem II (Micromeritics) equipped with a thermal conductivity detector (TCD). In a typical experiment, 35 mg of the calcined sample was firstly degassed at 200 °C for 30 min. H_2 gas flow (10 vol% H_2/Ar) was then introduced and the sample was heated from 50 °C to 950 °C at a heating rate of 10 °C/min.

The adsorption–desorption isotherms of N_2 at −196 °C was measured using Tristar II 3020 (Micromeritics) instrument. The monolithic sample was degassed at 150 °C overnight prior to the analysis. The surface area was then calculated using the Brunauer-Emmet-Teller (BET) equation [21] while the pore volume was estimated using the Barrett-Joyner-Halenda (BJH) method [22].

The morphology and elemental mapping of the catalytic layers were characterized with scanning electron microscopy (SEM), Gemini SUPRA 35VP (Carl Zeiss Jena) equipped with EDAX energy dispersive X-ray spectroscopy (EDS). For better image analysis, the monolithic samples were polished using very fine SiC abrasive grits. After cleaning with ethanol and drying, the samples were then coated with Pd to inhibit charging.

The inductive coupled plasma optical emission spectrometry (ICP-OES) method was applied to analyze the elemental compositions of dried LDHs precursors. The samples were dissolved in chloric acid and nitric acid prior to analysis by Optima 4300 DV (PerkinElmer) instrument.

2.3. Catalytic activity tests and temperature profile studies

CO_2 methanation tests were performed in a stainless steel structured reactor (inner diameter of 21.1 mm) heated by an electric tubular oven. An in-house designed catalyst holder (inner diameter of 19.1 mm) was used so that the monolith could be inserted inside the reactor without any gas channeling or flow bypass effect.

The catalytic performance of individual monolithic catalyst was carried out at a total gas flow of 500 mL/min (STP), corresponding to a GHSV of 7760 h^{-1}. The ratio of $H_2/N_2/CO_2$ in the gas mixture was 64/20/16 vol% (i.e., H_2/CO_2 = 4/1). Temperature-programmed reaction was conducted from 200 to 500 °C at ambient pressure with a temperature step of 50 °C. The temperature was controlled by a type-K thermocouple installed inside the reactor at the gas inlet. Prior to the reaction, the monolithic catalyst was in-situ reduced at 600 °C for 4 h in flowing H_2 gas (50 vol% H_2/N_2, 200 mL/min, STP).

For the study of temperature profiles along the catalytic bed, a multi-point thermocouple (Watlow) was installed to measure temperatures at 6 different positions, as illustrated in Fig. 1. The catalytic bed contained three monoliths with a total length of 60 mm. The monoliths were drilled through at the center (hole diameter of 3 mm) so that the multi-point thermocouple could be inserted. The temperature of the oven was controlled by another thermocouple (T_{oven}) located outside of the reactor. The temperature of the gas inlet was also monitored by the thermocouple at the gas inlet (T_{gas_in}). The reaction temperature was varied from 200 to 300 °C at ambient pressure with different gas flow rates of up to 3000 mL/min (STP). The stability test was carried out at T_{oven} of 250 °C at a gas flow rate of 1500 mL/min (STP) for 100 h.

At the reactor gas outlet, a cold trap was used to remove water formed during reaction before the outgases were introduced into the online gas chromatograph (GC 7890A, Agilent) for analysis. A blank test of the pure honeycomb substrate was conducted, and no catalytic conversion was observed. The CO_2 conversion (X_{CO2}), CH_4 yield (Y_{CH4}), and CH_4 productivity (P_{CH4}) were defined in Eqs. (2), (3), (4), where F^{in} and F^{out} are the molar flow rates in and out of the reactor (mol/h).

$$X_{CO2}(\%) = \frac{F^{in}_{CO2} - F^{out}_{CO2}}{F^{in}_{CO2}} \times 100 \quad (2)$$

$$Y_{CH4}(\%) = \frac{F^{out}_{CH4}}{F^{in}_{CO2}} \times 100 \quad (3)$$

$$P_{CH4}\left(mol/h.g_{cat}\right) = \frac{F^{out}_{CH4}}{m_{cat}} \quad (4)$$

2.4. CFD model development

Numerical simulations were developed to verify the thermal profiles along the monolithic beds obtained from experimental studies. A discretized three-dimensional (3D) computational geometry of one-eighth of a monolith with the same dimensions as lab-scale experiments was built (Fig. 2), which consisted of channel blocks and porous walls. Governing equations of the CFD models are reaction rate, continuity, momentum, mass, and energy equations as described in detail in Table S1 in the supporting information. All boundary conditions and parameters are listed in Table S2 and S3. The equations were solved by finite element based multiphysics simulation software COMSOL Multiphysics® version 5.5.

The model presents channels in monolithic reactor with a pseudo-homogeneous approach. The reaction rate and equilibrium equation were adapted from Koschany *et al.* [23,24]. The fluid flow was assumed as a fully developed laminar flow with weak compressibility, and the average gas velocity was set at the inlet. The temperature-dependent transport properties of the multicomponent gas mixtures (heat capacity, thermal conductivity, and viscosity) were automatically calculated by the software with a mass-fraction weighted rule. The gas diffusivity was estimated using Fuller-Schettler-Giddings equations while the effective binary diffusion coefficients in the porous walls were calculated with the Bruggeman correction model [25–27]. Atmospheric pressure was applied, and the pressure drop was neglected. The energy equation defines the reacting gas temperature in the channels and conductive heat transfer in the wall structure. The gas mixture was set at desired inlet temperature and heat generated from the reaction was the main heat source, while the ambient temperature was set as the oven temperature. Moreover, no-slip conditions were also applied together with a symmetric boundary condition since the modeling domain was reduced to one-eighth of the full reactor geometry.

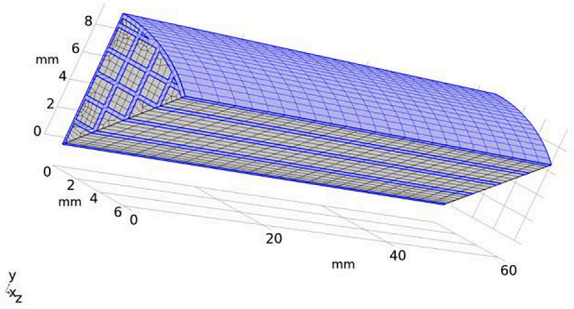

Fig. 2. Discretized one-eighth of the full monolithic reactor geometry; the structured mesh has 13296 elements.

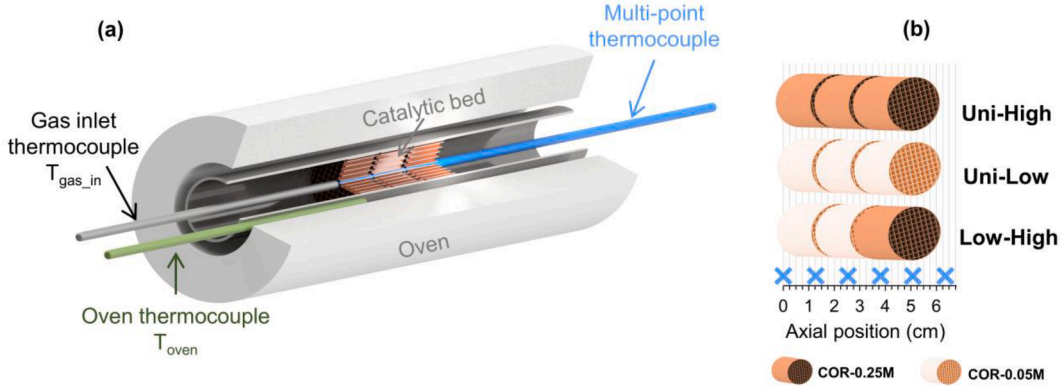

Fig. 1. (a) Illustration of upgraded structured reactor setup for temperature profile studies. (b) The axial position of measuring points by the multi-point thermocouple with respect to the gas inlet position of three different bed packing configurations, i.e., Uni-High, Uni-Low, and Low-High.

3. Results and discussion

3.1. Characterization of NiFe-CO_3 LDHs prepared at different metal concentrations

The influence of total metal concentrations during urea hydrolysis on the synthesis of as-prepared precursors was revealed by XRD analysis. The XRD diffractograms of dry precursors (Fig. 3) showed that highly crystalline LDHs materials were formed by using metal concentrations of up to 1M. Characteristic peaks of LDHs structures were observed for all samples except for LDH-2M, e.g., symmetric and sharp reflections at 2 of 11.5°, 23.3°, and 34.5° could be ascribed to the basal (003), (006), (012) planes, respectively (NiFe-CO_3 LDHs, JCPDS 00–051-0463). LDH-0.25M has the best crystallinity thus probably the most perfect LDH structure. As for LDH-2M, the precursor was amorphous since no diffraction peaks were observed. It has been reported that LDHs synthesized at high metal concentrations had poorer crystallinity [28]. Moreover, to form a pure LDHs structure, the Fe^{3+}/Ni^{2+} molar ratio should be in the range of 0.2–0.33 [29–31]. However, at high Fe^{3+} concentrations, it was more favorable for Fe^{3+} ion to precipitate as insoluble $Fe(OH)_3$ in aqueous ammonia [32]. Indeed, the elemental analysis via ICP-OES showed that precursors prepared at metal concentrations above 1M had high Fe content compared with the nominal value (Table S4 in the supporting information). Therefore, it can be concluded that 0.25M was the most ideal metal concentration to prepare NiFe-CO_3 LDHs.

Upon calcination at 600 °C, it was expected that a mixed metal oxide of Ni and Fe would form from LDHs precursors [20]. The diffractograms of the calcined LDHs were presented in Fig. 4. It confirmed that LDHs structures were completely decomposed since only the diffraction patterns of $NiFe_2O_4$ (JCPDS 00-054-0964) and NiO (JCPDS 01-089-5881) were identified. It can also be observed that the XRD pattern of the calcined LDH-2M showed mostly reflections of $NiFe_2O_4$ due to higher Fe content compared to the other samples.

The reducibility of the calcined catalysts was investigated by H_2-TPR analysis (Fig. 5). With increasing metal concentrations, the main reduction temperature of the metal oxides was increased. It has been reported that pure NiO could be reduced at 340–410 °C and Fe_2O_3 is reduced sequentially at 380, 620, and 715 °C [33,34]. In this study, the TPR peaks of calcined LDH-0.05M, LDH-0.25M and LDH-0.5M were at 415, 430 and 485 °C, respectively. It is reasonable that the reduction temperature of Ni species would be increased due to the interaction with Fe species in the mixed oxides [35]. As for LDH-1M and LDH-2M samples, small reduction peaks were observed at 310–330 °C which could be attributed to the reduction of NiO, while the main peaks were recorded at high temperatures of 540–545 °C. It was in good agreement with the previous assumption that these two samples contained more iron oxides.

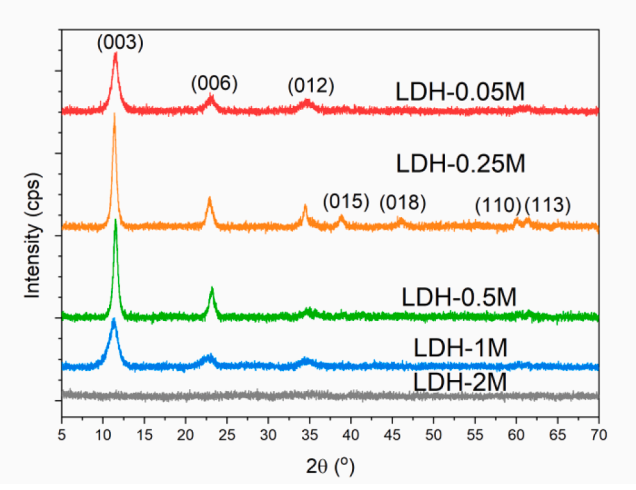

Fig. 3. XRD diffractograms of NiFe-CO_3 LDHs prepared by urea hydrolysis at different metal concentrations.

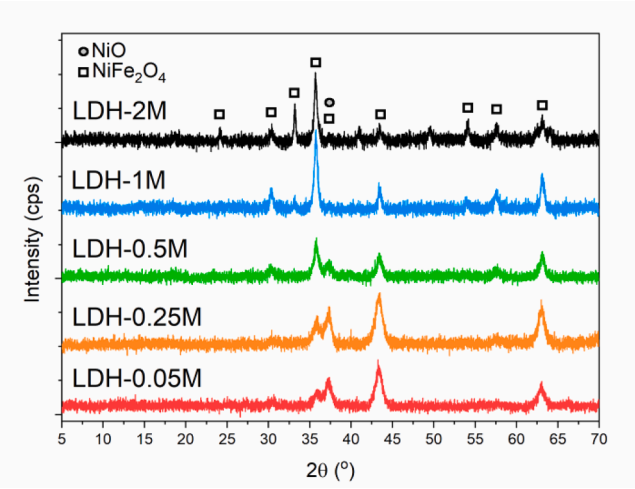

Fig. 4. XRD diffractograms of the calcined NiFe-CO_3 LDHs.

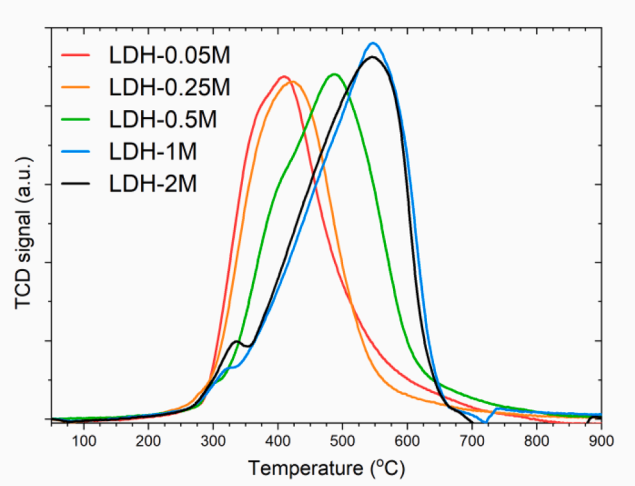

Fig. 5. TPR profiles of calcined NiFe-CO_3 LDHs.

3.2. Characterization of monolithic catalysts

The NiFe-CO_3 LDHs layer was in-situ grown on the washcoated honeycomb ceramic substrate via urea hydrolysis at different metal concentrations from 0.05M to 2M. The amount of deposited LDHs layers on the monoliths as well as catalyst loading are summarized in Table 1. Noted that the catalyst loading was calculated as the percentage of the catalyst mass after calcination on the total weight of final monoliths. It

Table 1
The mass of in-situ grown LDHs, corresponding catalyst loading and textural properties of the final calcined monolithic catalysts.

Structured catalysts	Mass of LDHs (mg)	Catalyst loading (wt %)	BET specific surface area ($m^2/g_{total\ COR}$)	BJH pore volume (cm^3/g)
COR-0.05M	60.1	0.52	18.3	0.047
COR-0.25M	192.9	3.51	24.4	0.051
COR-0.5M	175.8	2.63	30.7	0.069
COR-1M	168.3	1.87	22.6	0.047
COR-2M	163.5	1.12	18.6	0.047

was found that the highest amount of LDHs precursor could be deposited on monolith prepared at metal concentration of 0.25M. It is also the sample with the most crystalline LDHs structure. Thus, increasing metal concentrations could not increase the amount of in-situ grown LDHs precursors on washcoated substrate. As discussed in the XRD analysis, the formation of pure and high crystalline LDH structure was not favored at metal concentrations above 1M.

Cordierite honeycomb substrate is one of the most popular materials for the synthesis of structured catalysts thanks to its availability and low costs. However, cordierite substrate originally has a very low surface area, which was 1.2 m^2/g in our study. Thus, the substrate was washcoated with colloidal alumina three times to reach a washcoat layer loading of 14 wt%. After calcination, the washcoated monolith had a higher surface area of 18.3 m^2/g and pore volume of 0.064 cm^3/g. The surface area and pore volume of final monoliths after urea hydrolysis are summarized in Table 1. It shows that the surface area was significantly improved after urea hydrolysis, especially for monolith prepared at 0.25M, 0.5M and 1M.

The morphology of catalytic layer deposited on cordierite monoliths upon urea hydrolysis was observed by SEM. Numerous hexagonal platelets of LDHs were found on the exterior wall of the monolithic channels, in good agreement with earlier studies [36]. As shown in Fig. 6, the lateral size and thickness of these platelets on COR-0.25M and COR-1M were around 1 μm and 25 ± 10 nm. The morphology of LDHs precursors on COR-0.05M was almost three-time smaller in lateral size (Fig. S1a), while the platelet dimensions of COR-0.25M, COR-0.5M and COR-1M (Figs. 6 and S1b) was similar.

The thickness of the catalytic layer was estimated using the cross-sectional SEM images of the channel wall. As shown in Fig. 7, the deposition of LDHs occurred on the porous exterior of the cordierite channel walls. The LDHs platelets were assumed to grow perpendicularly on the surface, resulting in a layer thickness of around 20–30 μm. Notably, the catalytic layer on COR-0.25M, COR-0.5M, and COR-1M had similar thicknesses (Fig. 7 and Fig. S1d). As for COR-0.05M, it was unable to measure the LDHs layer due to very low catalyst loading (Fig. S1c). In addition, EDS elemental mapping was conducted and revealed a uniform spatial distribution of Ni and Fe on the layer, indicating that the metal ions were well dispersed on the monolithic surface.

3.3. Catalytic performance of monolithic catalysts

The temperature-programmed reaction was carried out at 200–500 °C for all monolithic catalysts. Due to kinetic limitations, high conversion of CO_2 could not be obtained at low temperature region of 200–250 °C, even though CO_2 methanation is thermodynamically favored. The conversion was much improved at 300 °C, especially for COR-0.25M monolith which achieved a CO_2 conversion of 70.1% (Fig. 8). COR-0.5M and COR-1M also exhibited good activity at 300 °C with CO_2 conversion of 65.6% and 59.6%, respectively. The conversions peaked at 350 °C and gradually decreased at elevated temperatures, following the thermodynamic equilibrium. On the other hand, COR-0.05M showed a poorer performance, and COR-2M presented the poorest activity.

In addition to the main reaction, the reverse water gas shift reaction (RWGS, $CO_2 + H_2 \leftrightarrow CO + H_2O$, $\Delta H_{298K} = 41$ kJ/mol) could occur to produce the byproduct CO. Hence, the CH_4 selectivity or CH_4 yield is also an important indicator for the performance of the catalysts. In this study, CH_4 yield is reported together with the loading of catalysts (Fig. 9). The best performance of COR-0.25M amongst others was confirmed by the CH_4 yield at different reaction temperatures. This could be due to the highest catalyst loading of COR-0.25M with a thin and well-adhered layer on the honeycomb substrate. Interestingly, CO_2 conversion over the COR-2M catalyst was always increasing with temperature, distinct from the other catalysts as it did not follow the thermodynamic curve for methanation. This could be explained by the high Fe content of COR-2M, which promotes the endothermic RWGS reaction and favors CO_2 conversion at high temperatures [37]. Indeed, the CH_4 selectivity was very low over the COR-2M monolith.

3.4. Temperature profiles of structured reactor

3.4.1. Temperature profiles with increasing oven temperatures

The exothermic nature of the methanation reaction could be influenced by different catalytic activities of the monolithic catalysts. Thus, the temperature along the catalytic bed containing high and low activity catalysts (COR-0.25M and COR-0.05M, respectively) was measured by the multi-point thermocouple at the center of the bed. At first, the reaction was carried out on uniform catalytic beds containing three COR-0.25M monoliths (Uni-High bed) or three COR-0.05M monoliths (Uni-Low bed). Fig. 10 shows the temperature profile and the methane yield of the catalytic beds at steady state when T_{oven} was 200, 250 and 300 °C, respectively.

At T_{oven} = 200 °C and a total gas flow rate of 500 mL/min, the CH_4 yield on both monolithic beds was relatively low at less than 3.5% (Fig. 10a). As expected, no hot-spot formation was observed from the axial temperature profiles. When the oven temperature ramped up to 250 °C (Fig. 10b), hot-spot appeared along the Uni-High bed with a maximum temperature increase (ΔT) of 42 °C in the middle of the bed. The catalytic performance also improved with a CH_4 yield of 50.9%. In contrast, a CH_4 yield of only 8.9% was achieved on the Uni-Low bed, and there was obviously no hot-spot formation at this low conversion. When T_{oven} was increased from 250 to 300 °C, the hot-spot on Uni-High bed shifted from the center axial position to near the gas inlet region with a significant ΔT = 86 °C, whereas the CH_4 yield increased to 84.1% (Fig. 10c). A CH_4 yield of 59.5% was achieved on the Uni-Low bed at T_{oven} = 300 °C, and hot-spot was also observed with ΔT = 44 °C. The thermal profile of catalytic beds could result from the balance between the exothermic heat from methanation which increased exponentially with reaction temperature due to reaction rate acceleration, and heat transfer by conduction in the cordierite channel wall and by convection from the bed to the gas flow. The shift of hot-spot location at increasing operating temperature has also been reported by Kosaka *et al.* [17]. It

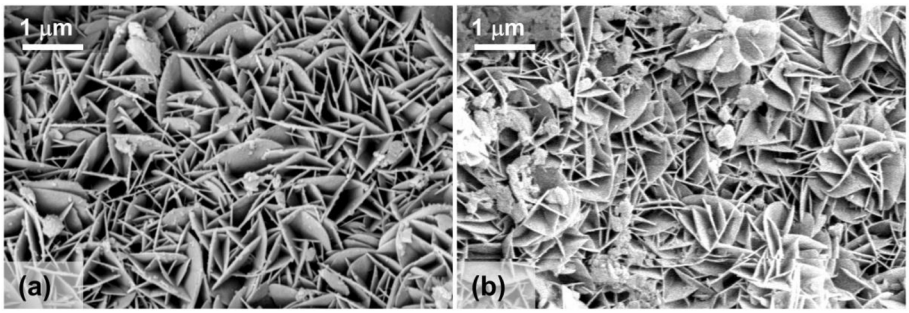

Fig. 6. SEM images of in-situ grown NiFe-CO_3 LDHs on (a) COR-0.25M and (b) COR-1M monolith.

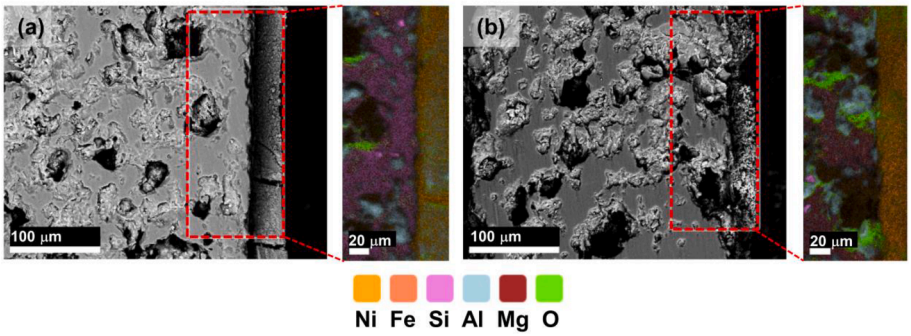

Fig. 7. SEM and corresponding EDS elemental mapping images of the cross-sectional channel wall on (a) COR-0.25M and (b) COR-1M.

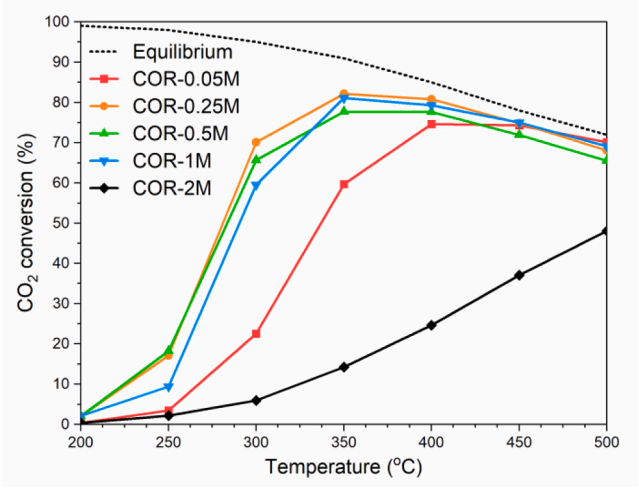

Fig. 8. CO_2 conversion over structured catalysts in temperature-programmed CO_2 methanation at atmospheric pressure, total gas flow rate of 500 mL/min (STP), $H_2/N_2/CO_2$ = 64/20/16 vol%; The thermodynamic equilibrium was added for comparison.

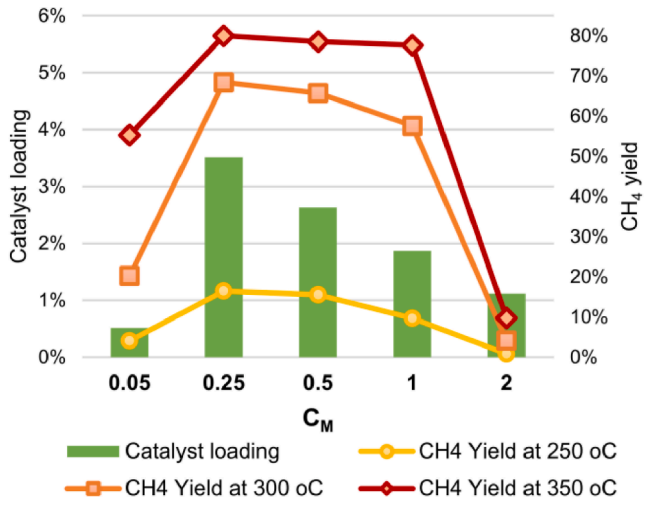

Fig. 9. CH_4 yield obtained over structured catalysts at different reaction temperatures (200, 250 and 300 °C); The CO_2 methanation reaction was at atmospheric pressure, total gas flow rate of 500 mL/min (STP), $H_2/N_2/CO_2$ = 64/20/16 vol%.

could be due to the higher heat conductivity of the catalytic cordierite monolith bed compared to that of the flowing gas. Thus, heat transfer along the monolithic bed was faster than that between the catalytic bed and the gas. Subsequently, monolith at the near gas inlet was further heated and accelerated methanation reactions. Simultaneously, a large amount of exothermic reaction heat was released.

It was proposed that the excellent thermal conductivity of monolithic substrate could be utilized to boost up the performance of low activity catalysts in methanation [17]. We therefore configured a monolithic bed with increasing catalytic activity, i.e., Low-High bed consisting of two COR-0.05M and one COR-0.25M. Hot-spot was not observed at T_{oven} = 200 °C (Fig. 10a) but was measured with ΔT = 26 °C and a CH_4 yield of 32.1% at T_{oven} = 250 °C. Notably, at T_{oven} = 300 °C, the CH_4 yield of the Low-High bed was almost close to that of the Uni-High bed (83.1% vs 84.1%) while a lower ΔT of 69 °C was recorded. Thus, although the Low-High bed contained less catalyst loading than the Uni-High bed, the CH_4 yield was almost similar at T_{oven} = 300 °C. As shown in Fig. 8, while COR-0.25M slowly dropped its performance at 350 °C and above, the CO_2 conversion over COR-0.05M still increased and reached a maximum at 400–450 °C. It seems that hot-spot generated in the reaction could be exploited to improve the overall performance of the Low-High bed. In terms of methane productivity when catalyst mass was taken into account, P_{CH4} was 0.9 mol/(h.g_{cat}) on Uni-High and 1.6 mol/(h.g_{cat}) on Low-High bed. Hence, it can be assumed that the Low-High bed packing strategy could enhance the catalytic efficiency of the monolithic reactor with a lower hot-spot temperature.

3.4.2. CFD simulation results

The experimental results for all three catalytic beds were verified by a 3D CFD consisted of reaction kinetics, fluid dynamics, heat transfer and mass transport. The simulated temperature profiles at a gas inlet temperature of 250 °C along three catalytic beds (Fig. 11) showed similar patterns of hot-spot formation compared to the experimental results at T_{oven} = 250 °C (Fig. 10b). The simulation demonstrated that the highest temperature of 290 °C on Uni-High bed was at the middle of the bed (Fig. 11a), while on Low-High bed the maximum temperature T_{max} of 258 °C was detected at the third monolith COR-0.25M near the gas outlet (Fig. 11c). As expected, the temperature profile of the Uni-Low bed was quite flat without any hot-spot formation (Fig. 11b). Thus, the proposed bed packing strategy by combining catalysts with low and high activity appeared to be a promising approach to manage bed temperatures.

3.4.3. Temperature profiles with increasing gas flow rates

We further studied the effect of GHSV on the catalytic conversion and temperature profile of Uni-High and Low-High beds at T_{oven} = 250 °C (Fig. 12). For comparison, the CH_4 yield and temperature profile at 500 mL/min were also included as Fig. 12a. The hot-spot formation was more pronounced at higher gas flow rate of 1500 mL/min (corresponding to a GHSV of 7760 h^{-1}). The Uni-High bed reached a T_{max} of 458 °C with a remarkable CH_4 yield of 80.4% (Fig. 12b). It is worth emphasizing that the ratio of the catalyst mass to volumetric gas flow rate was the same for the single-bed at 500 mL/min and Uni-High bed at

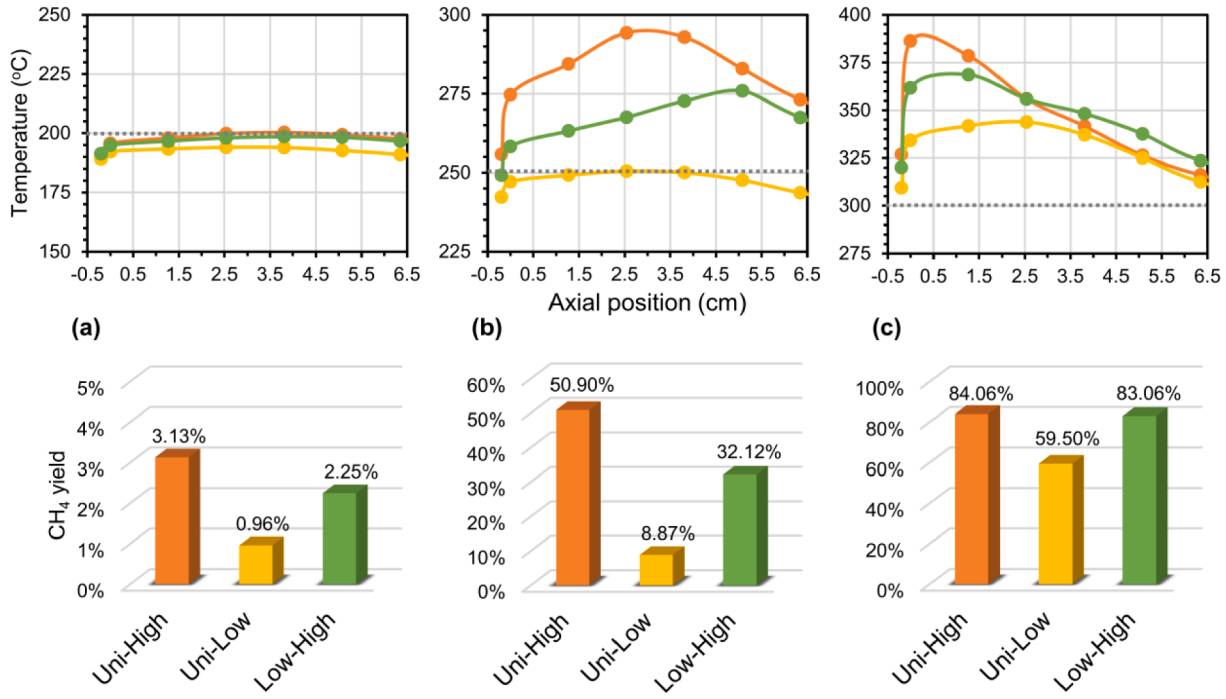

Fig. 10. Temperature profiles of reactor (top) and methane yield (bottom) obtained from CO_2 methanation over different catalytic beds at T_{oven} of (a) 200 °C, (b) 250 °C, (c) 300 °C; The reaction was at atmospheric pressure, total gas flow rate of 500 mL/min (STP), $H_2/N_2/CO_2$ = 64/20/16 vol%.

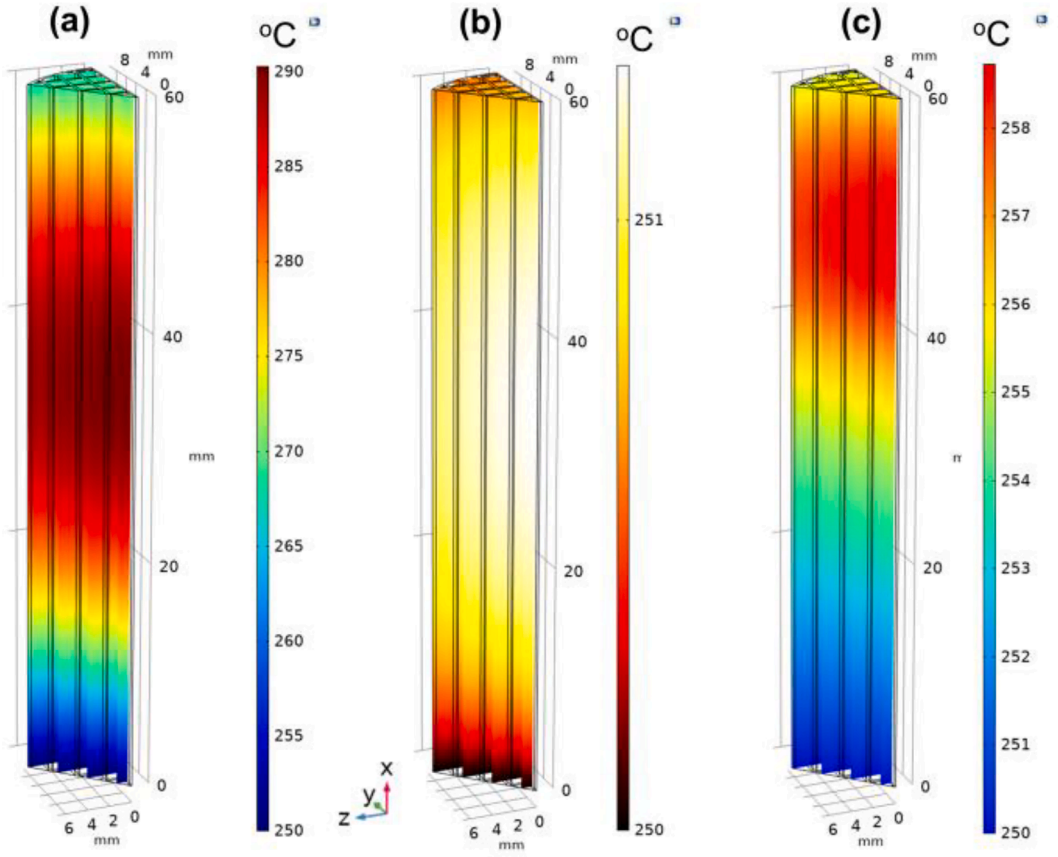

Fig. 11. Simulated temperature profiles of monolithic reactor using (a) Uni-High, (b) Uni-Low and (c) Low-High bed at operating temperature of 250 °C, atmospheric pressure, total gas flow rate of 500 mL/min (STP).

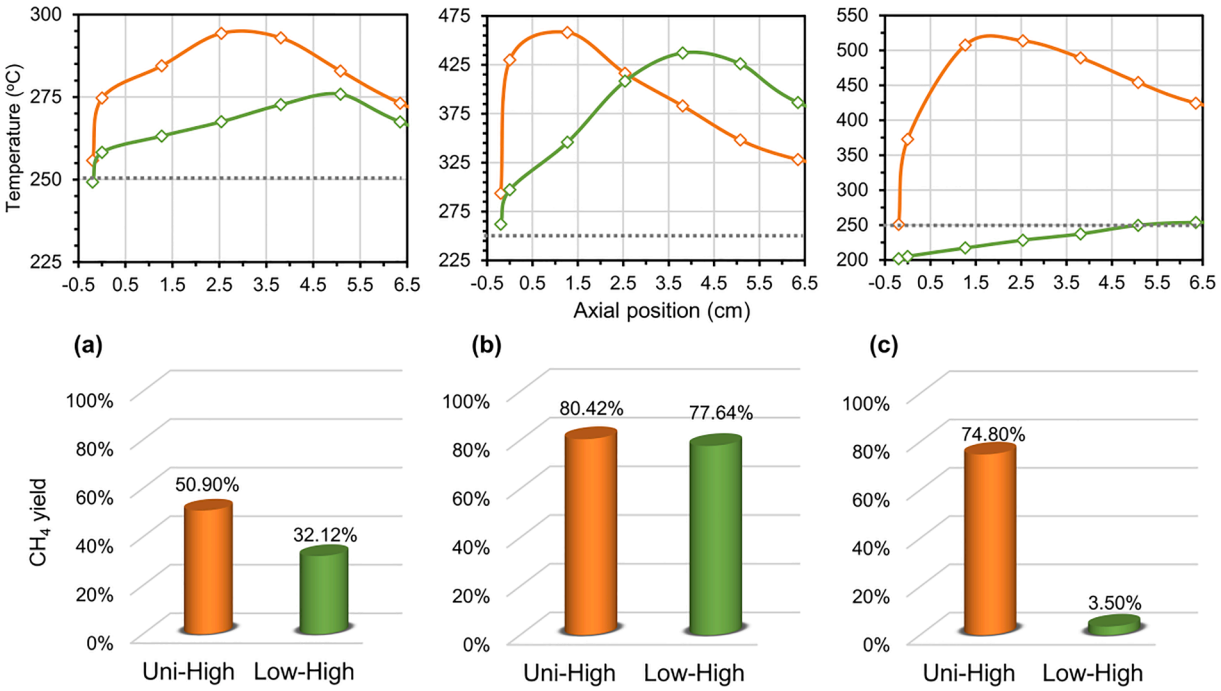

Fig. 12. Temperature profiles of reactor (top) and methane yield (bottom) obtained from CO_2 methanation over Uni-High and Low-High bed at different gas flow rates of (a) 500 mL/min, (b) 1500 mL/min and (c) 3000 mL/min (STP). The temperature of the oven was set at 250 °C. The reaction was at atmospheric pressure, $H_2/N_2/CO_2$ = 64/20/16 vol%.

1500 mL/min, whereas the CH_4 yield was only 16.5% for the former (Fig. 9). Obviously, the hot-spot generated on the Uni-High bed had significantly boosted the overall CH_4 yield to 80.4%. Thus, while hot-spot formation is a big concern for many chemical reactions [18], it could also be utilized to boost the performance of exothermic monolithic reactors. As for the Low-High bed, it showed a lower T_{max} of 437 °C at a gas flow rate of 1500 mL/min while the CH_4 yield was only marginally lower at 77.6%, apparently due to the hot-spot formed on the reactor bed. The strategic Low-High packing was again demonstrated to be a promising alternative to the uniform Uni-High bed.

Lower CO_2 conversion and CH_4 yield are generally expected at higher GHSV at the same reaction temperature. Interestingly, the catalytic performance of both monolithic beds was significantly improved at a higher gas rate of 1500 mL/min compared to 500 mL/min. This could also be explained by the hot-spot observed in the reactor: the initial CO_2 conversion was probably lower at 1500 mL/min, but the amount of heat released and the heat transfer coefficient would be larger at higher flow rate, which increased the bed temperature thus further accelerated the reaction. Consequently, the monolithic bed was operated at a much higher temperature at 1500 mL/min than that at 500 mL/min, as shown in Fig. 12a and Fig. 12b.

We also investigated the reactor performance at 3000 mL/min at T_{oven} = 250 °C. For Uni-High bed, a higher T_{max} of 513 °C, corresponding to a ΔT of 263 °C could be observed, whereas the CH_4 yield decreased to 74.8%. Indeed, a larger amount of heat was released at 3000 mL/min which led to a higher temperature spike. However, at 450–500 °C, COR-0.25M exhibited a lower conversion of only 75–68% (Fig. 8). As for the Low-High bed, the CH_4 yield was merely 3.5%. The residence time at this condition could be too short for the two low-activity COR-0.05M catalytic beds, thus CO_2 was not reacted and no heat was released to form hot-spot (Fig. 12c). To sum up, at a very high gas flow of 3000 mL/min, extreme hot-spot formation was not favorable for the conversion on Uni-High bed while it was too harsh condition for Low-High bed to produce methane.

3.4.4. Stability tests

Long-term stability test was carried out on both Uni-High and Low-High beds at T_{oven} = 250 °C and a gas flow rate of 1500 mL/min (STP). The T_{max} on Low-High bed was maintained at 440 °C during the 100-h long-term test. On Uni-High bed, the high hot-spot temperature was slightly decreased from 468 to 460 °C, which could be explained by the loss of activity during 100 h. Regardless, it was consistent with previous tests that Low-High bed had a lower hot-spot compared to that of Uni-High bed (Fig. 13). This could also explain the lower but more stable methane yield with a slight drop of 0.02%/h on the Low-High bed compared to a deactivation rate of 0.05%/h on the Uni-High bed. Nevertheless, both bed configurations have shown quite stable performance throughout 100 h of reaction. Therefore, CO_2 methanation could be effectively carried out on monolithic reactors at a very low operating temperature of 250 °C.

4. Conclusions

NiFe catalytic active layer was in-situ grown on washcoated ceramic substrate via urea hydrolysis, which is a novel preparation method to obtain thin and well-adhered catalytic layer on monoliths. It was found that catalysts prepared by 0.25M solution, i.e., COR-0.25M with the highest metal loading exhibited the best CO_2 conversion and CH_4 yield. The formation of hot-spot during exothermic methanation reaction was observed on monolithic reactors and further verified by CFD simulations. Although a temperature increase of 86 °C was observed on Uni-High bed reactor, a remarkable methane yield of 80.4% was achieved at low operating temperature of 250 °C. In contrast, the methane yield was merely 16.5% on single COR-0.25M bed at this temperature. Therefore, controlled hot-spot formation was beneficial for the overall catalytic performance via bed packing. A strategic bed packing configuration was proposed that combined low and high activity monolith, i.e., Low-High bed. Amazingly, this bed achieved ~83% methane yield and the hot-spot formation was less severe compared to that of the Uni-High bed at 300 °C. It was also revealed that hot-spot formation could be exploited to achieve high methane yield at high gas flow rate during

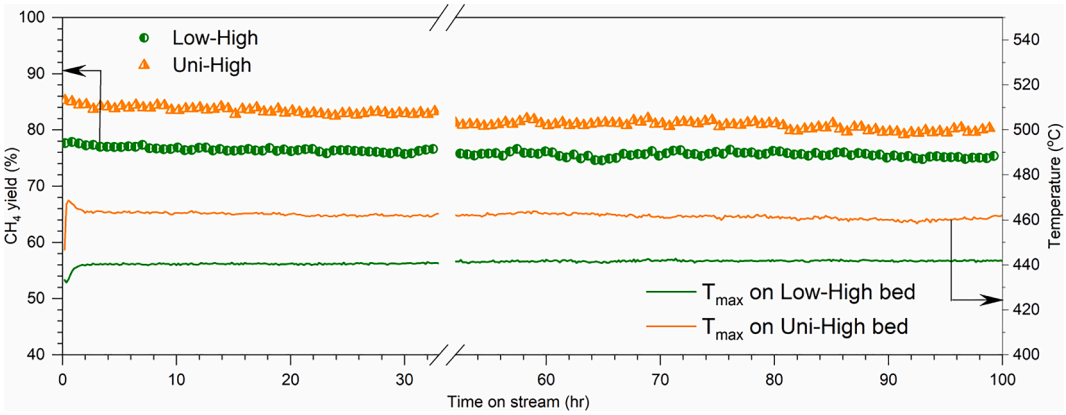

Fig. 13. Methane yield and maximum temperature of the Low-High and Uni-High bed during long-term tests. The oven temperature was set at 250 °C. The reaction was at atmospheric pressure, total gas flow rate of 1500 mL/min (STP), $H_2/N_2/CO_2$ = 64/20/16 vol%.

low-temperature CO_2 methanation on honeycomb monolithic reactors. In conclusion, hot-spot and strategic bed packing could be utilized to achieve excellent CO_2 methanation performance on monolithic reactors at low temperatures. These results demonstrated a promising approach for the development of industrial monolithic CO_2 methanation reactors as part of large-scale PtG process.

Declaration of Competing Interest

The authors declare that they have no known competing financial interests or personal relationships that could have appeared to influence the work reported in this paper.

Acknowledgments

The authors would like to thank the Norwegian Ministry of Education and Research for the financial support.

Appendix A. Supplementary data

Supplementary data to this article can be found online at https://doi.org/10.1016/j.cej.2021.131106.

References

[1] J. Artz, T.E. Müller, K. Thenert, J. Kleinekorte, R. Meys, A. Sternberg, A. Bardow, W. Leitner, Sustainable conversion of carbon dioxide: an integrated review of catalysis and life cycle assessment, Chem. Rev. 118 (2) (2018) 434–504, https://doi.org/10.1021/acs.chemrev.7b00435.

[2] P. Sabatier, J.-B. Senderens, Nouvelles syntheses du methane, Comptes Rendus Des Séances De L'Académie Des Sciences, Section VI – Chimie 134 (1902) 514–516.

[3] C. Vogt, M. Monai, G.J. Kramer, B.M. Weckhuysen, The renaissance of the sabatier reaction and its applications on earth and in space, Nat. Catal. 2 (3) (2019) 188–197, https://doi.org/10.1038/s41929-019-0244-4.

[4] M. Götz, J. Lefebvre, F. Mörs, A. McDaniel Koch, F. Graf, S. Bajohr, R. Reimert, T. Kolb, Renewable power-to-gas: a technological and economic review, Renew. Energy 85 (2016) 1371–1390, https://doi.org/10.1016/j.renene.2015.07.066.

[5] M. Bailera, P. Lisbona, L.M. Romeo, S. Espatolero, Power to gas projects review: Lab, pilot and demo plants for storing renewable energy and CO2, Renew. Sustain. Energy Rev. 69 (2017) 292–312, https://doi.org/10.1016/j.rser.2016.11.130.

[6] C. Lv, L. Xu, M. Chen, Y. Cui, X. Wen, Y. Li, C.-E. Wu, B. Yang, Z. Miao, X. Hu, Q. Shou, Recent progresses in constructing the highly efficient ni based catalysts with advanced low-temperature activity toward co2 methanation, Front. Chem. 8 (269) (2020), https://doi.org/10.3389/fchem.2020.00269.

[7] P. Frontera, A. Macario, M. Ferraro, P. Antonucci, Supported catalysts for co2 methanation: a review, Catalysts 7 (2) (2017) 59, https://doi.org/10.3390/catal7020059.

[8] D. Türks, H. Mena, U. Armbruster, A. Martin, Methanation of CO2 on Ni/Al2O3 in a structured fixed-bed reactor—a scale-up study, Catalysts 7 (5) (2017) 152, https://doi.org/10.3390/catal7050152.

[9] A. Bengaouer, J. Ducamp, I. Champon, R. Try, Performance evaluation of fixed-bed, millistructured, and metallic foam reactor channels for CO2 methanation, Can. J. Chem. Eng. 96 (9) (2018) 1937–1945, https://doi.org/10.1002/cjce:23140.

[10] M. Lehner, R. Tichler, H. Steinmüller, M. Koppe, Methanation, in: M. Lehner, R. Tichler, H. Steinmüller, M. Koppe (Eds.), Power-to-gas: technology and business models, springer international publishing, Cham, 2014, pp. 41–61, https://doi.org/10.1007/978-3-319-03995-4_4.

[11] F. Kapteijn, J.A. Moulijn, Structured catalysts and reactors – perspectives for demanding applications, Catal. Today (2020), https://doi.org/10.1016/j.cattod.2020.09.026.

[12] C. Fukuhara, K. Hayakawa, Y. Suzuki, W. Kawasaki, R. Watanabe, A novel nickel-based structured catalyst for CO2 methanation: a honeycomb-type Ni/CeO2 catalyst to transform greenhouse gas into useful resources, Appl. Catal. A 532 (2017) 12–18, https://doi.org/10.1016/j.apcata.2016.11.036.

[13] H.L. Huynh, Z. Yu, CO2 Methanation on hydrotalcite-derived catalysts and structured reactors: a review, Energy Technol. 8 (5) (2020) 1901475, https://doi.org/10.1002/ente.201901475.

[14] S. Hwang, P. Linke, R. Smith, Heterogeneous catalytic reactor design with optimum temperature profile II: application of non-uniform catalyst, Chem. Eng. Sci. 59 (20) (2004) 4245–4260, https://doi.org/10.1016/j.ces.2004.05.036.

[15] S. Ratchahat, M. Sudoh, Y. Suzuki, W. Kawasaki, R. Watanabe, C. Fukuhara, Development of a powerful CO2 methanation process using a structured Ni/CeO2 catalyst, J. CO2 Util. 24 (2018) 210–219, https://doi.org/10.1016/j.jcou.2018.01.004.

[16] F. Kosaka, T. Yamaguchi, Y. Ando, T. Mochizuki, H. Takagi, K. Matsuoka, K. Kuramoto, Thermal management of CO2 methanation with axial staging of active metal concentration in Ni-YSZ tubular catalysts, Int. J. Hydrog. Energy 46 (5) (2020) 4116–4125, https://doi.org/10.1016/j.ijhydene.2020.10.247.

[17] F. Kosaka, T. Yamaguchi, Y. Ando, T. Mochizuki, H. Takagi, K. Matsuoka, Y. Fujishiro, K. Kuramoto, Effect of Ni content on CO2 methanation performance with tubular-structured Ni-YSZ catalysts and optimization of catalytic activity for temperature management in the reactor, Int. J. Hydrog. Energy 45 (23) (2020) 12911–12920, https://doi.org/10.1016/j.ijhydene.2020.02.221.

[18] W. Wang, C. Duong-Viet, G. Tuci, Y. Liu, A. Rossin, L. Luconi, J.-M. Nhut, L. Nguyen-Dinh, G. Giambastiani, C. Pham-Huu, Highly nickel-loaded γ-alumina composites for a radiofrequency-heated, low-temperature co2 methanation scheme, ChemSusChem 13 (20) (2020) 5468–5479, https://doi.org/10.1002/cssc.202001885.

[19] J. Jenkins, E. Shutt, The hot spot™ reactor, Platinum Met. Rev. 33 (3) (1989) 118–127.

[20] H.L. Huynh, W.M. Tucho, Z. Yu, Structured NiFe catalysts derived from in-situ grown layered double hydroxides on ceramic monolith for CO2 methanation, Green Energy Environ. 5 (4) (2020) 423–432, https://doi.org/10.1016/j.gee.2020.09.004.

[21] S. Brunauer, P.H. Emmett, E. Teller, Adsorption of gases in multimolecular layers, J. Am. Chem. Soc. 60 (2) (1938) 309–319, https://doi.org/10.1021/ja01269a023.

[22] E.P. Barrett, L.G. Joyner, P.P. Halenda, The Determination of pore volume and area distributions in porous substances. I. computations from nitrogen isotherms, J. Am. Chem. Soc. 73 (1) (1951) 373–380, https://doi.org/10.1021/ja01145a126.

[23] F. Koschany, D. Schlereth, O. Hinrichsen, On the kinetics of the methanation of carbon dioxide on coprecipitated NiAl(O)x, Appl. Catal. B 181 (2016) 504–516, https://doi.org/10.1016/j.apcatb.2015.07.026.

[24] G. Tauer, C. Kern, A. Jess, Transient effects during dynamic operation of a wall-cooled fixed-bed reactor for co2 methanation, Chem. Eng. Technol. 42 (11) (2019) 2401–2409, https://doi.org/10.1002/ceat.201900367.

[25] E.N. Fuller, P.D. Schettler, J.C. Giddings, New method for prediction of binary gas-phase diffusion coefficients, Ing. Eng. Chem. 58 (5) (1966) 18–27, https://doi.org/10.1021/ie50677a007.

[26] E.N. Fuller, K. Ensley, J.C. Giddings, Diffusion of halogenated hydrocarbons in helium. The effect of structure on collision cross sections, J. Phys. Chem 73 (11) (1969) 3679–3685.

[27] T. Fuller, Proton exchange membrane fuel cells 8, Electrochem. Soc. (2008).

[28] Z. Chang, D.G. Evans, X. Duan, C. Vial, J. Ghanbaja, V. Prevot, M. de Roy, C. Forano, Synthesis of [Zn–Al–CO3] layered double hydroxides by a

coprecipitation method under steady-state conditions, J. Solid State Chem. 178 (9) (2005) 2766–2777, https://doi.org/10.1016/j.jssc.2005.06.024.
[29] M.V. Bukhtiyarova, A review on effect of synthesis conditions on the formation of layered double hydroxides, J. Solid State Chem. 269 (2019) 494–506, https://doi.org/10.1016/j.jssc.2018.10.018.
[30] F. Cavani, F. Trifirò, A. Vaccari, Hydrotalcite-type anionic clays: preparation, properties and applications, Catal. Today 11 (2) (1991) 173–301, https://doi.org/10.1016/0920-5861(91)80068-K.
[31] V. Rives, María Angeles Ulibarri, Layered double hydroxides (LDH) intercalated with metal coordination compounds and oxometalates, Coord. Chem. Rev 181 (1) (1999) 61–120.
[32] N.J. Tro, Chemistry A Molecular Approach, Pearson, 2003.
[33] D. Pandey, K. Ray, R. Bhardwaj, S. Bojja, K.V.R. Chary, G. Deo, Promotion of unsupported nickel catalyst using iron for CO2 methanation, Int. J. Hydrog. Energy 43 (10) (2018) 4987–5000, https://doi.org/10.1016/j.ijhydene.2018.01.144.
[34] D. Beierlein, D. Häussermann, M. Pfeifer, T. Schwarz, K. Stöwe, Y. Traa, E. Klemm, Is the CO2 methanation on highly loaded Ni-Al2O3 catalysts really structure-sensitive? Appl. Catal. B 247 (2019) 200–219, https://doi.org/10.1016/j.apcatb.2018.12.064.
[35] D. Shi, R. Wojcieszak, S. Paul, E. Marceau, Ni promotion by Fe: what benefits for catalytic hydrogenation? Catalysts 9 (5) (2019) 451, https://doi.org/10.3390/catal9050451.
[36] Y. Han, H. Li, X. Ma, Z.-H. Liu, Preparation and formation process of Ni2+–Fe3+ CO32− LDHs materials with high crystallinity and well-defined hexagonal shapes, Solid State Sci. 11 (12) (2009) 2149–2155, https://doi.org/10.1016/j.solidstatesciences.2009.08.016.
[37] C.-S. Chen, W.-H. Cheng, S.-S. Lin, Study of iron-promoted Cu/SiO2 catalyst on high temperature reverse water gas shift reaction, Appl. Catal. A 257 (1) (2004) 97–106, https://doi.org/10.1016/S0926-860X(03)00637-9.